Finite element formulation of fluctuating hydrodynamics for fluids filled with rigid particles using boundary fitted meshes

M. De Corato*

Dipartimento di Ingegneria Chimica, dei Materiali e della Produzione Industriale, Università di Napoli Federico II, Piazzale Tecchio 80, 80125 Napoli, Italy

J.J.M. Slot

Department of Mathematics and Computer Science, Eindhoven University of Technology, PO Box 513, 5600 MB Eindhoven, The Netherlands

M. Hütter

Department of Mechanical Engineering, Eindhoven University of Technology, PO Box 513, 5600 MB Eindhoven, The Netherlands

G. D'Avino

Dipartimento di Ingegneria Chimica, dei Materiali e della Produzione Industriale, Università di Napoli Federico II, Piazzale Tecchio 80, 80125 Napoli, Italy

P.L. Maffettone

Dipartimento di Ingegneria Chimica, dei Materiali e della Produzione Industriale, Università di Napoli Federico II, Piazzale Tecchio 80, 80125 Napoli, Italy

M.A. Hulsen

Department of Mechanical Engineering, Eindhoven University of Technology, PO Box 513, 5600 MB Eindhoven, The Netherlands

Abstract

---

*Corresponding author. +39 0817682280; fax +39 0812391800

Email addresses: marco.decorato@unina.it (M. De Corato), j.j.m.slot@tue.nl (J.J.M. Slot), m.huetter@tue.nl (M. Hütter), gadavino@unina.it (G. D'Avino), pierluca.maffettone@unina.it (P.L. Maffettone), m.a.hulsen@tue.nl (M.A. Hulsen)

In this paper, we present a finite element implementation of fluctuating hydrodynamics with a moving boundary fitted mesh for treating the suspended particles. The thermal fluctuations are incorporated into the continuum equations using the Landau and Lifshitz approach [1]. The proposed implementation fulfills the fluctuation-dissipation theorem exactly at the discrete level. Since we restrict the equations to the creeping flow case, this takes the form of a relation between the diffusion coefficient matrix and friction matrix both at the particle and nodal level of the finite elements. Brownian motion of arbitrarily shaped particles in complex confinements can be considered within the present formulation. A multi-step time integration scheme is developed to correctly capture the drift term required in the stochastic differential equation (SDE) describing the evolution of the positions of the particles.

The proposed approach is validated by simulating the Brownian motion of a sphere between two parallel plates and the motion of a spherical particle in a cylindrical cavity. The time integration algorithm and the fluctuating hydrodynamics implementation are then applied to study the diffusion and the equilibrium probability distribution of a confined circle under an external harmonic potential.

Key words: Fluctuating hydrodynamics, Brownian motion, Finite element method, Stokes equation, Numerical simulations

1. Introduction

When dealing with the motion of submicron particles suspended in fluids, the Brownian motion arising from the thermal fluctuations becomes impor-

tant. Diffusion is, indeed, relevant in colloidal suspensions, biological processes both at the cell and the sub-cell level [2], and in several microfluidic applications [3, 4], in microrheology to determine local properties of complex fluids through the particle motion [5].

Many methods have been developed to simulate the Brownian motion of particles suspended in liquids. The conventional approach is to impose the fluctuating forces directly on the particles. Brownian dynamics simulation is surely one of the most used numerical methods whereby a modified Langevin equation is solved [6]. The Stokesian dynamics technique by Brady and Bossis [7] also falls in this category. Although this method is highly successful for simulation of Newtonian suspensions, its application to more complex fluids, inertial effects, irregular shaped and/or flexible particles is difficult, if not impossible. For example, in a recent paper, De Corato et al. [8] employed finite element simulations to compute the mobility of a spheroidal particle near a wall. However, the application of this method to more complex systems, like suspensions of many particles, is difficult. The main reason is that at the particle level the fluctuating forces are determined by the full drag coefficient matrix where all hydrodynamic interactions between particles have been taken into account. This makes the problem tractable only for the Stokes equations and for regular shaped particles, like spheres.

Instead of imposing the stochastic forces directly on the particles, it is possible to add thermal fluctuations to the fluid and let the fluid generate the fluctuating forces on the particles. Landau and Lifshitz [1] introduced the concept of a stochastic stress tensor, to incorporate such thermal fluctuations into the continuum equations. The equations of Landau and Lifshitz

3

fulfill the fluctuation dissipation theorem (FDT) at the continuum level. The resulting equations of fluctuating hydrodynamics, however, are difficult to directly incorporate in a standard discretization scheme, such as the finite element method. Indeed, in order to have the correct level of thermal fluctuations at all resolved scales, the FDT must be fulfilled at the discrete level. Though required, in general, after discretization, the FDT is likely to be violated [9] [10].

Several numerical approaches have been proposed for including thermal fluctuations in a macroscopic fluid flow solver using fluctuating hydrodynamics. Patankar [11] simulated for the first time in two dimensions the thermal motion of a particle suspended in a quiescent fluid medium using the fluctuating hydrodynamics approach in a finite element method (FEM). A Lagrangian implementation has been employed, but no details on the implementation of the fluctuating forces are given. The first finite volume discretization based on FDT arguments was reported by Atzberger et al. [12], simulations using a fixed grid finite volume method [10] and the Lattice-Boltzmann method [13] have also been carried out. Serrano et al. adopted a Lagrangian finite volume discretization using Voronoi cells [14]. The latter scheme uses the GENERIC formalism [15] [16] at the discrete level instead of a discretization of the continuum description of Landau and Lifshitz, ensuring that the FDT is obeyed. Bell et al. [17] discuss an implementation of the fluctuating hydrodynamics formulation of Landau and Lifshitz in a one-dimensional and three dimensional [18] compressible flow solver. It turns out that the well-known traditional discretizations are unable to accurately reproduce the correct fluctuations in energy and density and special tempo-

ral and spatial discretizations are required. Donev et al. [19] showed, in a finite volume context, that, in order to correctly capture the field fluctuations, a skew-adjoint relation between the discretized gradient and divergence operators is required, and the covariance of discrete force field has to be proportional to the discretized Laplacian operator.

More recently, Uma et al. [20] solved the fluctuating hydrodynamics equations by a finite element method to simulate the Brownian motion of a spherical nanoparticle suspended in a Newtonian fluid confined in a cylindrical vessel. They accounted for both particle and fluid inertial terms as well as fluid compressibility. The discrete hydrodynamics equations were obtained by using finite element shape functions based on the Delaunay-Voronoi tetrahedrization. The mesh deformations due to the particle movements inside the computational domain is handled through an ALE scheme. The authors find that, to obtain the correct particle velocity distribution, an additional non-Markovian process has to be added to the particle equation of motion [21, 22].

Finite volume [9] [23] [24] [12], spectral [25] or finite difference [26] implementations of the fluctuating hydrodynamics have been proposed for numerical simulations of particle suspensions; fluid-structure interactions are taken into account through immersed boundary or force coupling methods. While these methods present a convenient computational scaling with the number of particles the hydrodynamics interactions are only accurate up to the leading order of the multipole expansion (or up to the stresslet term) and more importantly are only valid for Newtonian suspending fluids. While all the above mentioned papers [9, 23, 24, 12, 25, 26] employ a regular grid to discretize the

spatial domain, recently Plunkett et al. [27] proposed a spatially adaptive fluctuating hydrodynamics FEM discretization, where the fluid structure interactions are taken into account through an immersed boundary method. In order to generate the correct stochastic forcing fields in the discretized domain, an iterative procedure is employed by the authors.

In this paper, we present a moving boundary fitted mesh finite element implementation of the fluctuating hydrodynamics. We demonstrate that our implementation fulfills the fluctuation-dissipation theorem exactly at the discrete level. Since we restrict the equations to the creeping flow case (Stokes equations), this will take the form of a relation between the diffusion coefficient matrix and friction matrix both at the particle and nodal level of the finite elements. In contrast to what reported in [27], in the implementation in this paper we directly generate the correct stochastic forcing fields, whereas these are only approximated by an iterative procedure in [27]. We emphasize that, in the present implementation, fluid-structure hydrodynamics interactions are captured to controlled accuracy, whereas only approximated methods have been employed in literature [9] [23] [24] [25] [12] [26] [10]. Hence, the present method allows numerical simulations of the Brownian motion of arbitrarily shaped particles in complex confinements, although at a higher computational cost compared to the computational cost of approximate methods.

In the absence of any particle inertia, the stochastic differential equation governing the dynamics of the suspended particles configuration requires an additional corrective term proportional to the spatial derivatives of the particle diffusion tensor [28]; this term has been, typically, called drift term.

6

The presence of such a stochastic drift term in the SDE is essential to obtain a particle equilibrium distribution matching that given by the Boltzmann distribution [29]. In this paper we present a multi-step time integration algorithm that circumvents the explicit calculation of the drift term, speeding up calculations that are otherwise very cumbersome. In our manuscript, as an illustrative example and, in order to verify the results more easily, we restrict the analysis to spherical particles, where we dont have the additional difficulty of the orientation dependency of quantities. We recognize that algorithms for arbitrarily shaped bodies have been recently proposed [30]. Application of our time integration algorithm to arbitrary particle shape as well as numerical optimization of the proposed algorithm, following recently developed ideas [9, 31], will be object of further work.

The proposed method is applied to simulate the Brownian motion of a spherical particle between two parallel walls and in a cylindrical cavity. Finally, the fluctuating hydrodynamics is applied to study the equilibrium distribution of a confined circle in an external potential.

The paper is organized as follows. In Section 2, we present the governing equations for the flow of a fluid filled with rigid particles experiencing random thermal fluctuations. In Section 3, we derive a weak form of the governing equations and present the numerical implementation of the fluctuating forces. We will also show that the fluctuation-dissipation relation is fulfilled at the discrete level. In Section 4, we present the time integration scheme required to correctly reproduce the drift term and our moving mesh algorithm. In Section 5, we present our numerical results for the Brownian motion of a sphere under confinement and for a confined circle under

7

an external potential. Finally, conclusions and future work are discussed in Section 6.

2. Governing equations

We will consider the flow of incompressible Newtonian fluids at very low Reynolds numbers. Therefore inertia will be neglected, and the flow is described by the Stokes equations. The fluctuating forces in the fluid are modeled using the concept of fluctuating hydrodynamics of Landau & Lifshitz [1] (see also [32] and [33]), in which these forces are represented by fluctuating stresses. Particle inclusions are assumed to be rigid, and the inertia of the particles will be neglected as well.

2.1. Stokes equations with fluctuating hydrodynamics

We consider the Stokes equations in a region Ω with an additional stochastic term on the right-hand side according to [1]:

$$-\nabla \cdot (2\eta \boldsymbol{D}) + \nabla p = \boldsymbol{f} + \nabla \cdot \boldsymbol{s}, \qquad \text{in } \Omega \tag{1}$$

$$-\nabla \cdot \boldsymbol{u} \qquad\qquad = 0 \qquad\qquad \text{in } \Omega \tag{2}$$

Here, $\boldsymbol{u}$ is the velocity vector, p is the pressure, η is the viscosity of the fluid, $\boldsymbol{D} = (\nabla \boldsymbol{u} + \nabla \boldsymbol{u}^T)/2$, $\boldsymbol{f}$ is a body force and $\boldsymbol{s}$ is the fluctuating stress tensor. For an incompressible Newtonian fluid the fluctuating stress tensor $\boldsymbol{s}$ is assumed to be uncorrelated in space and time, and to have a Gaussian distribution characterized by the following moments [1, 33]:

$$\langle \boldsymbol{s} \rangle = \boldsymbol{0} \tag{3}$$

$$\langle s_{\alpha\beta}(\boldsymbol{x}, t) s_{\gamma\nu}(\boldsymbol{x}', t') \rangle = 2k_{\mathrm{B}} T \eta (\delta_{\alpha\gamma}\delta_{\beta\nu} + \delta_{\alpha\nu}\delta_{\beta\gamma}) \delta(\boldsymbol{x} - \boldsymbol{x}') \delta(t - t') \tag{4}$$

where k_B is Boltzmann's constant and T is the absolute temperature. Note, that we use Greek symbols (α, β, γ and ν) to denote component directions of vectors and tensors. The fluctuating stresses are chosen in such a way that they fulfill the fluctuating-dissipation theorem at the continuum level.

The boundary Γ will be split into a Dirichlet (Γ_D) and a Neumann part (Γ_N) and the following set of boundary conditions are assumed

$$\boldsymbol{u} = \boldsymbol{u}_D \text{ on } \Gamma_D \tag{5}$$

$$-p\boldsymbol{n} + 2\eta \boldsymbol{D} \cdot \boldsymbol{n} + \boldsymbol{s} \cdot \boldsymbol{n} = \boldsymbol{t}_N \text{ on } \Gamma_N \tag{6}$$

where $\boldsymbol{n}$ is the outwardly directed unit normal vector. The Neumann condition is equivalent to an imposed traction $\boldsymbol{t}_N$.

The equations (1)–(2) can only be interpreted in an 'integrated' or distributional sense. The stochastic stress $\boldsymbol{s}$ is delta-correlated in space and time and is a rather singular object: the variance of $\boldsymbol{s}$ is infinite [34]. If we integrate $\boldsymbol{s}$ (for example the s_{12} component) over a small space-time domain $\Delta x \times \Delta y \times \Delta z \times \Delta t$ we get

$$\int_{\Delta x \times \Delta y \times \Delta z \times \Delta t} s_{12}(\boldsymbol{x}, t) \, dx dy dz dt = 2k_B T \eta \Delta W \tag{7}$$

with

$$\langle \Delta W^2 \rangle = \Delta x \Delta y \Delta z \Delta t \tag{8}$$

Hence ΔW can be seen as a multi-dimensional Wiener increment, which has a clear interpretation. A non-rigorous way to express s_{12} could then be

$$s_{12} = 2k_B T \eta \frac{\partial^4 W}{\partial x \partial y \partial z \partial t} \tag{9}$$

with $W(\boldsymbol{x}, t)$ a multi-dimensional Wiener process, but it should be noted that derivatives of a Wiener process do not exist [34].

Similar to $\boldsymbol{s}$, the pressure field p is also delta-correlated (in space and time) and can only be interpreted in an integrated sense. Therefore, only after integration over time *and* over a surface (2D) or a volume (3D) of the pressure field p mesh converging properties (like the variance) may be expected. The velocity field $\boldsymbol{u}$ is found by 'integrating twice' in space, so it is 'less singular' than $\boldsymbol{s}$ or p, but only by integrating in time *and* over a curve (2D) or a surface (3D) it will have mesh-converging properties (such as the variance).

In the original equations of Landau & Lifshitz [1] inertia is included and the delta-correlation in time is removed by the time-integration of the inertia term. In our Stokes formulation the delta-correlation in time remains and must be properly taken into account by time-integration using methods like Brownian dynamics [28].

2.2. Rigid particle boundary conditions

The equations (1) and (2) with boundary conditions (5) and (6) are insufficient to model rigid particle inclusions. A rigid particle condition is required at the fluid-particle interface.

In Fig. 1 the problem domain consists of a fluid domain (Ω) with external boundary Γ and internal (particle) boundaries $\Gamma_{\mathrm{p}i}$. The fluid-particle interface is part of the domain boundary and we assume the fluid adheres to the particle (no-slip), i.e. the velocity is given by

$$\boldsymbol{u} = \boldsymbol{U}_i + \boldsymbol{\omega}_i \times (\boldsymbol{x} - \boldsymbol{r}_i) \text{ on } \Gamma_{\mathrm{p}i} \tag{10}$$

where $\Gamma_{\mathrm{p}i}$ is the interface boundary corresponding to particle P_i, $i = 1 \ldots N_{\mathrm{p}}$, with N_{p} the number of particles.
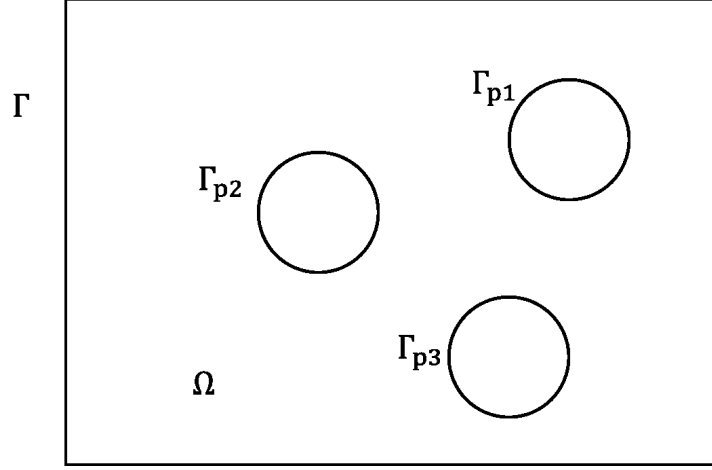
Figure 1: The fluid domain Ω with external boundary Γ and internal (particle) boundaries $\Gamma_{\mathrm{p}i}$. The external boundary can be split into a Dirichlet part (Γ_{D}) and Neumann part (Γ_{N}).

In these conditions $\boldsymbol{U}_i$ and $\boldsymbol{\omega}_i$ are unknown velocities and rotation rates of the particles, respectively, and $\boldsymbol{r}_i$ is the position of the particle that defines $\boldsymbol{U}_i$. In order to determine $(\boldsymbol{U}_i, \boldsymbol{\omega}_i)$ we need the additional condition that the sum of the forces and torques on each particle is zero since we have neglected inertia:

$$-\boldsymbol{F}_i + \boldsymbol{F}_i^{\mathrm{ext}} = \boldsymbol{0} \tag{11}$$

$$-\boldsymbol{M}_i + \boldsymbol{M}_i^{\mathrm{ext}} = \boldsymbol{0} \tag{12}$$

where $\boldsymbol{F}_i^{\mathrm{ext}}$ and $\boldsymbol{M}_i^{\mathrm{ext}}$ are external forces and torques acting on particle P_i. $\boldsymbol{F}_i$ and $\boldsymbol{M}_i$ are given by

$$\boldsymbol{F}_i = \int_{\Gamma_{\mathrm{p}i}} \boldsymbol{t}\,\mathrm{d}A \tag{13}$$

$$\boldsymbol{M}_i = \int_{\Gamma_{\mathrm{p}i}} (\boldsymbol{x} - \boldsymbol{r}_i) \times \boldsymbol{t}\,\mathrm{d}A \tag{14}$$

11

with $\boldsymbol{t}$ the traction vector *on the fluid*. Therefore, $\boldsymbol{F}_i$ and $\boldsymbol{M}_i$ are the force and torque on the fluid and $-\boldsymbol{F}_i$ and $-\boldsymbol{M}_i$ are the force and torque on the particle exerted by the fluid. Note, that

$$\boldsymbol{t} = -p\boldsymbol{n} + 2\eta \boldsymbol{D} \cdot \boldsymbol{n} + \boldsymbol{s} \cdot \boldsymbol{n} \tag{15}$$

where $\boldsymbol{n}$ is the outwardly directed unit normal vector on the *fluid* boundary.

As a final remark, it is worthwhile to mention that the governing equations (1), (2), (11) and (12) should be, in principle, derived from the full system of equations including both fluid and particle inertia and, then, considering the inertialess asymptotic limit as done in Tabak and Atzberger [35] in the immersed boundary context. Nevertheless, when both fluid and particle inertia are neglected, only the particle position dynamics 'survives', and the fluid velocity degrees of freedom only serve to generate the particle displacements. Indeed, the stochastic stress field could be chosen somewhat arbitrarily as long as it generates the correct particle displacements, that is to say, as long as the fluctuation-dissipation theorem holds at the particle level.

3. Weak form and numerical approximation

We need a weak form of the equations for obtaining an approximate solution within a finite element framework. Since the equations of fluctuating hydrodynamics can only be interpreted in an integrated form, the weak formulation is a natural framework to formulate the problem.

3.1. Weak form

First, we derive the weak form of the system Eqs. (1)–(2) without the rigid-body boundary conditions Eq. (10). The weak form can be obtained by multiplying Eqs. (1)–(2) with test functions $\boldsymbol{v}$ and q:

$$(\boldsymbol{v}, -\nabla \cdot \boldsymbol{\sigma} - \boldsymbol{f}) = 0, \qquad \text{for all } \boldsymbol{v} \tag{16}$$

$$-(q, \nabla \cdot \boldsymbol{u}) = 0, \qquad \text{for all } q \tag{17}$$

where

$$(\boldsymbol{a}, \boldsymbol{b}) = \int_{\Omega} \boldsymbol{a} \cdot \boldsymbol{b} \, \mathrm{d}V \tag{18}$$

$$(a, b) = \int_{\Omega} ab \, \mathrm{d}V \tag{19}$$

and $\boldsymbol{\sigma} = -p\boldsymbol{I} + 2\eta\boldsymbol{D} + \boldsymbol{s}$.

Using partial integration and Gauss' theorem we obtain the following weak form: Find $\boldsymbol{u}$ and p such that

$$\left(\boldsymbol{D}_v, 2\eta\boldsymbol{D}\right) - (\nabla \cdot \boldsymbol{v}, p) = (\boldsymbol{v}, \boldsymbol{t}_{\mathrm{N}})_{\Gamma_{\mathrm{N}}} + (\boldsymbol{v}, \boldsymbol{f}) - \left((\nabla\boldsymbol{v})^T, \boldsymbol{s}\right) \qquad \text{for all } \boldsymbol{v} \tag{20}$$

$$- (q, \nabla \cdot \boldsymbol{u}) = 0, \qquad\qquad\qquad \text{for all } q \tag{21}$$

using appropriate spaces for $\boldsymbol{u}$, p, $\boldsymbol{v}$ and q. In this equation $\boldsymbol{D}_v$ is defined by

$$\boldsymbol{D}_v = (\nabla\boldsymbol{v} + \nabla\boldsymbol{v}^T)/2 \tag{22}$$

and the bilinear operator $(\,,\,)$ for tensors is given by

$$(\boldsymbol{A}, \boldsymbol{B}) = \int_{\Omega} \boldsymbol{A} : \boldsymbol{B} \, \mathrm{d}V \tag{23}$$

The integration over the volume gives the stochastic term

$$I_v(t) = -\left((\nabla\boldsymbol{v})^T, \boldsymbol{s}\right) \tag{24}$$

13

a clear interpretation. For example, the contribution of the s_{12} component is

$$I_{12}(t) = -(\frac{\partial v_1}{\partial x_2}, s_{12}) = -\int_\Omega \frac{\partial v_1}{\partial x_2} s_{12} \, \mathrm{d}V \tag{25}$$

Using the stochastic properties of s_{12} from Eq. (4), the stochastic properties of $I_{12}(t)$ are:

$$\langle I_{12}(t) I_{12}(t') \rangle = \int_\Omega \int_\Omega \frac{\partial v_1}{\partial x_2}(\boldsymbol{x}) \frac{\partial v_1}{\partial x_2}(\boldsymbol{x}') \langle s_{12}(\boldsymbol{x}, t) s_{12}(\boldsymbol{x}', t') \rangle \, \mathrm{d}V \, \mathrm{d}V'$$
$$= 2k_\mathrm{B} T \eta \Big(\int_\Omega [\frac{\partial v_1}{\partial x_2}]^2 \, \mathrm{d}V \Big) \delta(t - t') \tag{26}$$

which has a clear meaning, although it is still delta-correlated in time. Adding the contributions from all stress terms we get:

$$\langle I_v(t) I_v(t') \rangle = \int_\Omega \int_\Omega \left(\nabla \boldsymbol{v}(\boldsymbol{x}) \right)^T : \langle \boldsymbol{s}(\boldsymbol{x}, t) \boldsymbol{s}(\boldsymbol{x}', t') \rangle : \nabla \boldsymbol{v}(\boldsymbol{x}') \, \mathrm{d}V \, \mathrm{d}V'$$
$$= 4k_\mathrm{B} T \eta \Big(\int_\Omega (\nabla \boldsymbol{v})^T : \boldsymbol{D}_v \, \mathrm{d}V \Big) \delta(t - t') \tag{27}$$
$$= 4k_\mathrm{B} T \eta (\boldsymbol{D}_v, \boldsymbol{D}_v) \delta(t - t')$$

In order to impose the boundary conditions for the rigid particle, Eqs. (10), (13) and (14), we introduce the Lagrange multipliers $\boldsymbol{\lambda}_i$ on the particle boundary $\Gamma_{\mathrm{p}i}$ as unknowns in the system. Hence, in addition to the velocity $\boldsymbol{u}$ and pressure p fields, we have the unknowns $\boldsymbol{\lambda}_i$, $\boldsymbol{U}_i$ and $\boldsymbol{\omega_i}$ in the system. Correspondingly, we introduce the test functions $\boldsymbol{v}$, q, $\boldsymbol{\mu}_i$, $\boldsymbol{V}_i$, $\boldsymbol{\chi}_i$.

Now we state the following weak form: Find $\boldsymbol{u}$, p, $\boldsymbol{\lambda}_i$, $\boldsymbol{U}_i$, $\boldsymbol{\omega}_i$, $i = 1, \dots, N_\mathrm{p}$ such that

$$\left(\boldsymbol{D}_v, 2\eta\boldsymbol{D} \right) - (\nabla \cdot \boldsymbol{v}, p) + \sum_{i=1}^{N_\mathrm{p}} \left(\boldsymbol{v} - (\boldsymbol{V}_i + \boldsymbol{\chi}_i \times (\boldsymbol{x} - \boldsymbol{r}_i)), \boldsymbol{\lambda}_i \right)_{\Gamma_{\mathrm{p}i}} =$$

$$(\boldsymbol{v}, \boldsymbol{t}_\mathrm{N})_{\Gamma_\mathrm{N}} + (\boldsymbol{v}, \boldsymbol{f}) - \left((\nabla \boldsymbol{v})^T, \boldsymbol{s} \right) + \sum_{i=1}^{N_\mathrm{p}} \boldsymbol{V}_i \cdot \boldsymbol{F}_i^{\mathrm{ext}} + \sum_{i=1}^{N_\mathrm{p}} \boldsymbol{\chi}_i \cdot \boldsymbol{M}_i^{\mathrm{ext}} \tag{28}$$

14

$$-(q, \nabla \cdot \boldsymbol{u}) = 0 \tag{29}$$

$$\sum_{i=1}^{N_{\mathrm{p}}} \left(\boldsymbol{\mu}_i, \boldsymbol{u} - (\boldsymbol{U}_i + \boldsymbol{\omega}_i \times (\boldsymbol{x} - \boldsymbol{r}_i))\right)_{\Gamma_{\mathrm{p}i}} = 0 \tag{30}$$

for all $\boldsymbol{v}$, q, $\boldsymbol{\mu}_i$, $\boldsymbol{V}_i$, $\boldsymbol{\chi}_i$ and using appropriate spaces for $\boldsymbol{u}$, p, $\boldsymbol{v}$, q. The inner product $(\cdot, \cdot)_{\Gamma_{\mathrm{p}i}}$ on a particle boundary is given by:

$$(\boldsymbol{a}, \boldsymbol{b})_{\Gamma_{\mathrm{p}i}} = \int_{\Gamma_{\mathrm{p}i}} \boldsymbol{a} \cdot \boldsymbol{b} \, \mathrm{d}A \tag{31}$$

Notice that the total force and torque (Eqs. (13) and (14)) acting on the i-th particle are related to the Lagrange multipliers $\boldsymbol{\lambda}_i$ through:

$$\boldsymbol{F}_i = \int_{\Gamma_{\mathrm{p}i}} \boldsymbol{\lambda}_i \, \mathrm{d}A \tag{32}$$

$$\boldsymbol{M}_i = \int_{\Gamma_{\mathrm{p}i}} (\boldsymbol{x} - \boldsymbol{r}_i) \times \boldsymbol{\lambda}_i \, \mathrm{d}A \tag{33}$$

3.2. Numerical approximation using a Galerkin scheme

The weak form can be used to obtain an approximate solution using the Galerkin finite element technique. For this we divide the region Ω into elements:

$$\Omega = \cup_e \Omega_e, \quad \Omega_e \cap \Omega_{e'} = \emptyset \quad \text{for } e \neq e' \tag{34}$$

and interpolate $\boldsymbol{u}$ and p (and similarly $\boldsymbol{v}$ and q) by polynomials on each element:

$$\boldsymbol{u}_h = \sum_k \phi_k(\boldsymbol{x}) \boldsymbol{u}_k, \quad p_h = \sum_k \psi_k(\boldsymbol{x}) p_k \tag{35}$$

where $\phi_k(\boldsymbol{x})$ and $\psi_k(\boldsymbol{x})$ are global shape functions. The geometrical shape of the elements is determined by the velocity interpolation (isoparametric).

Before we define the numerical solution we need a procedure to compute the stochastic term:

$$I_v(t) = -\int_\Omega (\nabla \boldsymbol{v})^T : \boldsymbol{s}\, \mathrm{d}V \tag{36}$$

For this, we use the numerical integration scheme for the evaluation of the integrals in the usual finite element implementations:

$$\int_\Omega f(\boldsymbol{x})\, \mathrm{d}V \approx \sum_{m=1}^{N_\mathrm{g}} w_m f(\boldsymbol{x}_m) \tag{37}$$

where N_g is the number of integration points (for example using a Gauss integration scheme for each element), w_m is the weight in the integration point $\boldsymbol{x}_m$ and $f(\boldsymbol{x}_m)$ the value of the function in the integration point. Note, that w_m includes both the weights of the integration rule and the Jacobian of the mapping from the reference element to the real element shape. We assume $w_m \geq 0$, which is valid for all popular integration rules. Now we propose to compute the stochastic term in the following way. Introduce tensorial Gaussian stochastic processes $\boldsymbol{z}^m(t)$ (statistically independent between each integration point m) having the following moments:

$$\langle \boldsymbol{z}^m \rangle = \boldsymbol{0} \tag{38}$$

$$\langle z_{\alpha\beta}^m(t) z_{\gamma\nu}^n(t') \rangle = 2k_\mathrm{B}T\eta\delta_{mn}(\delta_{\alpha\gamma}\delta_{\beta\nu} + \delta_{\alpha\nu}\delta_{\beta\gamma})\delta(t - t') \tag{39}$$

Here m and n denote integration points. Now we compute an approximation of $I_v(t)$ by

$$\hat{I}_v(t) = -\sum_{m=1}^{N_\mathrm{g}} \sqrt{w_m}\big(\nabla \boldsymbol{v}(\boldsymbol{x}_m)\big)^T : \boldsymbol{z}^m(t) \tag{40}$$

The stochastic properties of $\hat{I}_v(t)$ are now the same as $I_v(t)$ up to the numer-

ical error of the integration rule:

$$\langle \hat{I}_v(t)\hat{I}_v(t')\rangle = \sum_{m=1}^{N_g}\sum_{n=1}^{N_g}\sqrt{w_m}\sqrt{w_n}\big(\nabla\boldsymbol{v}(\boldsymbol{x}_m)\big)^T : \langle \boldsymbol{z}^m(t)\boldsymbol{z}^n(t')\rangle : \nabla\boldsymbol{v}(\boldsymbol{x}'_n)$$

$$= 4k_\mathrm{B}T\eta\Big(\sum_{m=1}^{N_g}w_m(\nabla\boldsymbol{v}(\boldsymbol{x}_m))^T : \boldsymbol{D}_v(\boldsymbol{x}_m)\Big)\delta(t-t') \qquad (41)$$

$$= 4k_\mathrm{B}T\eta\Big(\sum_{m=1}^{N_g}w_m\boldsymbol{D}_v(\boldsymbol{x}_m) : \boldsymbol{D}_v(\boldsymbol{x}_m)\Big)\delta(t-t')$$

where we have used that $\boldsymbol{z}^m(t)$ fulfills the stochastic moments given by Eq. (39), which include the independence between integration points. Comparing Eq. (41) with Eq. (27) we see that the stochastic properties of $\hat{I}_v(t)$ are identical to $I_v(t)$ up to the error made in the numerical integration scheme.

In the practical implementation we take $\boldsymbol{z}^m(t)$ to be a symmetric tensor and thus need three (2D) or six (3D) random numbers in each integration point everytime the stochastic vector $\hat{I}_v(t)$ is generated. We use random numbers taken from a standard Gaussian distribution. We emphasize that our algorithm for the generation of the stochastic forcing fields only requires the generation of Gaussian random numbers, no iteration is required as in [27]; the computational cost of generating $\hat{I}_v(t)$ is $\mathcal{O}(N_e)$, with N_e the number of elements in which the spatial domain is discretized.

The weak form of the rigid body motion, Eq. (30), and similarly to the boundary term in Eq. (28), is approximated by point collocation:

$$\sum_{i=1}^{N_p}\big(\boldsymbol{\mu}_i, \boldsymbol{u}-(\boldsymbol{U}_i+\boldsymbol{\omega}_i\times(\boldsymbol{x}-\boldsymbol{r}_i))\big)_{\Gamma_{pi}} = \sum_{i=1}^{N_p}\sum_{k=1}^{N_{\mathrm{nod},i}}\boldsymbol{\mu}_{i,k}\cdot[\boldsymbol{u}(\boldsymbol{x}_k) - (\boldsymbol{U}_i + \boldsymbol{\omega}_i \times (\boldsymbol{x}_k - \boldsymbol{r}_i))]$$

$$(42)$$

where $N_{\mathrm{nod},i}$ are the number of the mesh nodal points on the i-th particle boundary, and $\boldsymbol{x}_k$ are the coordinates of the mesh point. Some remarks:

- The rigid body motion Eq. (10) is fulfilled exactly in the nodes on the particle boundary.

- The discrete form of equations for the forces and torques, Eqs. (32) and (33), on the boundary is given by:

$$\sum_{k=1}^{N_{\mathrm{nod}}} \boldsymbol{\lambda}_{i,k} = \boldsymbol{F}_i \tag{43}$$

$$\sum_{k=1}^{N_{\mathrm{nod}}} (\boldsymbol{x}_k - \boldsymbol{r}_i) \times \boldsymbol{\lambda}_{i,k} = \boldsymbol{M}_i \tag{44}$$

- The system is symmetric positive semi-definite.

We can now substitute the interpolations Eq. (35) into the weak form Eqs. (28)–(30), which leads to the following system of equations

$$\begin{bmatrix} S & L^T & M^T & 0 \\ L & 0 & 0 & 0 \\ M & 0 & 0 & N \\ 0 & 0 & N^T & 0 \end{bmatrix} \begin{bmatrix} u \\ p \\ \lambda \\ U \end{bmatrix} = \begin{bmatrix} f + \hat{I}(t) \\ 0 \\ 0 \\ g \end{bmatrix} \tag{45}$$

where u, p, λ and U are the system vectors for the velocity, pressure, particle nodal forces and particle motion unknowns (velocity $\boldsymbol{U}_i$ and rotation rate $\boldsymbol{\omega}_i$), g is the external force/torque vector conjugate to U (consisting of $\boldsymbol{F}_i^{\mathrm{ext}}$ and $\boldsymbol{M}_i^{\mathrm{ext}}$), the matrices L and M are the system matrices with respect to the incompressibility condition and particle motion, respectively. N is the matrix coupling the particle unknowns U to velocities on the particle boundary and the viscous system matrix S, the force vector f and the stochastic vector

$\hat{I}(t)$ are given by

$$S_{\alpha\beta}^{kl} = (\phi_{k,\gamma}, \eta\phi_{l,\gamma})\delta_{\alpha\beta} + (\phi_{l,\alpha}, \eta\phi_{k,\beta}) \tag{46}$$

$$f_\alpha^k = (\phi_k, t_{N\alpha})_{\Gamma_N} + (\phi_k, f_\alpha) \tag{47}$$

$$\hat{I}_\alpha^k(t) = -\sum_{m=1}^{N_g} \sqrt{w_m}\phi_{k,\gamma}(\boldsymbol{x}_m)z_{\gamma\alpha}^m(t) \tag{48}$$

using index notation with a summation convention for indices over coordinate directions and components of vectors and tensors. Here k and l denote nodal points. Formally we can combine both pressure p and λ into a single vector Λ and write Eq. (45) into a simplified form as follows

$$\begin{bmatrix} S & A^T & 0 \\ A & 0 & B \\ 0 & B^T & 0 \end{bmatrix} \begin{bmatrix} u \\ \Lambda \\ U \end{bmatrix} = \begin{bmatrix} f + \hat{I}(t) \\ 0 \\ g \end{bmatrix} \tag{49}$$

where $A^T = [L^T \ M^T]$ and $B^T = [0 \ N^T]$. In the present paper, in order to solve the linear system Eq. (49), which is the most time consuming step of our computations, we use the sparse direct solver PARDISO [36]. The simulations are performed in parallel using three cores. The use of more efficient iterative schemes, such as algebraic multigrid methods [37], to reduce the computational effort of solving Eq. (49) will be part of future investigation.

3.3. Fluctuation-dissipation relation for the discrete system

The fluctuating stresses in the theory of Landau & Lifshitz [1] are chosen in such a way as to fulfill the fluctuation-dissipation theorem at the continuum level. In this section we will show that the system Eq. (49) fulfills the fluctuation-dissipation relation at the *discrete* level for both the unknowns u

and U. In order to show that, we first need the stochastic properties of the stochastic vector $\hat{I}_\alpha^k(t)$, given by Eq. (48).

3.3.1. Properties of the stochastic vector $\hat{I}_\alpha^k(t)$

The covariance matrix of the vector $\hat{I}_\alpha^k(t)$ at two different time instants t and t' can be written as

$$
\begin{aligned}
\langle \hat{I}_\alpha^k(t)\hat{I}_\beta^l(t')\rangle &= \langle \sum_{m=1}^{N_\mathrm{g}} \sqrt{w_m}\phi_{k,\gamma}(\boldsymbol{x}_m)z_{\gamma\alpha}^m(t) \sum_{n=1}^{N_\mathrm{g}} \sqrt{w_n}\phi_{l,\nu}(\boldsymbol{x}_n)z_{\nu\beta}^n(t')\rangle \\
&= \sum_{m=1}^{N_\mathrm{g}}\sum_{n=1}^{N_\mathrm{g}} \sqrt{w_m}\sqrt{w_n}\phi_{k,\gamma}(\boldsymbol{x}_m)\phi_{l,\nu}(\boldsymbol{x}_n)\langle z_{\gamma\alpha}^m(t)z_{\nu\beta}^n(t')\rangle
\end{aligned}
\tag{50}
$$

Note, the use of the summation convection for the dummy indices γ and ν. Substitution of Eq. (39) gives:

$$
\begin{aligned}
\langle \hat{I}_\alpha^k(t)\hat{I}_\beta^l(t')\rangle &= \sum_{m=1}^{N_\mathrm{g}} w_m\phi_{k,\gamma}(\boldsymbol{x}_m)\phi_{l,\nu}(\boldsymbol{x}_m)\langle z_{\gamma\alpha}^m(t)z_{\nu\beta}^m(t')\rangle \\
&= \sum_{m=1}^{N_\mathrm{g}} w_m\phi_{k,\gamma}(\boldsymbol{x}_m)\phi_{l,\nu}(\boldsymbol{x}_m)2k_\mathrm{B}T\eta(\delta_{\gamma\nu}\delta_{\alpha\beta} + \delta_{\gamma\beta}\delta_{\alpha\nu})\delta(t-t') \\
&= 2k_\mathrm{B}T\delta(t-t') \sum_{m=1}^{N_\mathrm{g}} w_m(\phi_{k,\nu}\eta\phi_{l,\nu}\delta_{\alpha\beta} + \phi_{k,\beta}\eta\phi_{l,\alpha})_{\boldsymbol{x}_m} \\
&= 2k_\mathrm{B}T\delta(t-t')S_{\alpha\beta}^{kl}
\end{aligned}
\tag{51}
$$

where we used $()_{\boldsymbol{x}_m}$ to denote that the expression between the brackets must be evaluated at position $\boldsymbol{x}_m$. We have assumed that S has been computed with the *same numerical integration rule* as $\hat{I}(t)$. In matrix notation the equation for the covariance matrix of the vector $\hat{I}_\alpha^k(t)$ now becomes

$$
\langle \hat{I}(t)\hat{I}(t')^T\rangle = 2k_BTS\delta(t-t')
\tag{52}
$$

20

3.3.2. Discrete fluctuation-dissipation relations

By imposing only deterministic forces f on the system and without the complication of incompressibility and rigid body motion we have

$$u = S^{-1}f \tag{53}$$

The inverse resistance matrix is identified as $\zeta_u^{-1} = S^{-1}$. In the fluctuating system (with $f = 0$) we would have

$$u(t) = S^{-1}\hat{I}(t) \tag{54}$$

and thus with Eq. (52), we find

$$\langle u(t)u(t')^T \rangle = S^{-1}\langle \hat{I}(t)\hat{I}(t')^T \rangle S^{-1} = 2k_B T S^{-1}\delta(t - t') = 2k_B T \zeta_u^{-1}\delta(t - t') \tag{55}$$

Since (see Gardiner [34])

$$\langle u(t)u(t')^T \rangle = 2D_u \delta(t - t') \tag{56}$$

where D_u is the diffusion coefficient matrix, we find

$$D_u = k_B T \zeta_u^{-1} \tag{57}$$

i.e., the fluctuation-dissipation relation for the *discrete* system. As we do have the complication of incompressibility and rigid body motion, the proof is somewhat more elaborate, and can be found in Appendix A.

In Appendix A the system Eq. (49) is rewritten as

$$u = \zeta_u^{-1}f + \chi^T g \tag{58}$$

$$\Lambda = \kappa_u f + \kappa_U g \tag{59}$$

$$U = \chi f + \zeta_U^{-1}g \tag{60}$$

Note, that ζ_u is the resistance matrix for forces f directly on the nodes of the system, and ζ_U is the resistance matrix for forces/torques g on the particles.

The fluctuating system ($f = g = 0$, $\hat{I}(t) \neq 0$) can be found by substituting $\hat{I}(t)$ for f in the system above:

$$u = \zeta_u^{-1}\hat{I}(t) \tag{61}$$

$$\lambda = \kappa_u\hat{I}(t) \tag{62}$$

$$U = \chi\hat{I}(t) \tag{63}$$

In Appendix A it is shown that

$$\langle U(t)U(t')^T\rangle = 2k_BT\zeta_U^{-1}\delta(t - t') \tag{64}$$

and, therefore,

$$D_U = k_BT\zeta_U^{-1} \tag{65}$$

the fluctuation-dissipation relation holds for the *discrete* system with respect to the U vector (the particle level) as well, and takes the form of the Stokes-Einstein-Sutherland (SES) relation. Also

$$\langle u(t)u(t')^T\rangle = 2k_BT\zeta_u^{-1}\delta(t - t') \tag{66}$$

and therefore

$$D_u = k_BT\zeta_u^{-1} \tag{67}$$

Thus, the fluctuation-dissipation relation holds for the *discrete* system with respect to the u vector (the fluid velocity level).

It should be noted that Eq. (65) is a relation for the *discrete* system. If the finite element mesh is refined the resistance of the particle ζ_U will be more accurate and so will the fluctuation of the particle. For an infinitely refined mesh Eq. (65) will converge to the exact SES relation.

3.4. Choice of shape functions

All the standard compatible shape functions for velocity and pressure, such as the Taylor-Hood family (continuous pressure) and the Crouzeix-Raviart family (discontinuous pressure) can be used. Also higher-order elements (spectral or hp) are possible. For elements where the shape function for the velocity is a quadratic or a higher-order function, it is well-known that the resistance ('stiffness') of the inner nodes is different for each node (for quadratic interpolation the resistance of the mid-side node is higher than the vertex nodes). According to the SES relation Eq. (67) this also means that the variance of the fluctuating velocity field does not change smoothly from node to node (for quadratic interpolation the variance of the fluctuating velocity field is significantly less in the 'mid-side' nodes compared with the vertex nodes). This is not a problem if forces are also distributed in a 'consistent' manner, such as in Eq. (47) for the body force. In this work, we used triangular and tetrahedral elements having a continuous quadratic interpolation (P_2) for the velocity, and a continuous linear interpolation (P_1) for pressure. The P_2-P_1 interpolation for the velocity-pressure fields is known to satisfy the Babuška-Brezzi condition [38].

4. Time integration and Brownian drift

As a consequence of the fluctuating stress tensor, the suspended particles experience Brownian motion. Indeed, as shown by Fox and Uhlenbeck [32], the Eqs. (1) and (2) together with the freely moving particle condition Eqs. (10)-(12) give rise to a stochastic differential equation for the generalized particles positions vector r, containing all the particles positions and rota-

tions. In general, due to the hydrodynamic interaction with boundaries and other particles, the particle diffusion matrix $D_U(r) = k_B T \zeta_U^{-1}(r)$ depends on the instantaneous particle configuration $r(t)$. Such dependence gives rise to a corrective term in the Itô-interpreted SDE [28] that is linear in the time increment, i.e. it is a deterministic drift term, and proportional to the divergence of the particle diffusion matrix with respect to the particle configuration (positions and rotations). This additional term, as it contains spatial derivatives of the diffusion matrix, represents a (weakly) non-local drift; it's presence in the SDE is crucial to obtain a particle equilibrium distribution that matches the Boltzmann distribution [29, 28].

In this subsection, we propose a time integration algorithm for the particle trajectories $r(t)$ which correctly reproduces the additional drift term by a two-step scheme, rather than calculating it explicitly in a time-consuming way. We only consider spherical or circular particles for which the diffusion and resistance matrix depend on the positions only, therefore it is not required to update the particle rotations. We do however recognize that the tools for considering the Brownian motion of an arbitrarily shaped rigid body have been developed [30].

The Itô stochastic differential equation (SDE) for the generalized particle positions vector $r(t)$, in the overdamped limit, is given by [28]:

$$d\, r\,(t) = \sqrt{2 k_B T} \zeta_U^{-1}\,(r)\, \zeta_U^{\frac{1}{2}}\,(r)\, dW + \zeta_U^{-1}\,(r)\, F^{\text{ext}}(r)\, dt + k_B T \,\text{div}_r\, \zeta_U^{-1}\,(r)\, dt \tag{68}$$

In the above equation dW is the increment of a vectorial Wiener process [28], $F^{\text{ext}}(r)$ is a generalized force vector (i.e. containing the external forces and torques), div_r is the divergence with respect to the particle positions, and

24

the matrix $\zeta_U^{\frac{1}{2}}(r)$ satisfies the property:

$$\zeta_U^{\frac{1}{2}}(r)\left(\zeta_U^{\frac{1}{2}}(r)\right)^T = \zeta_U(r) \tag{69}$$

A forward discretization (i.e. Euler-Maruyama) of Eq. (68), would require the computation of the divergence of the mobility matrix $\zeta_U^{-1}(r)$, which is computationally very expensive.

Different predictor-corrector time integration algorithms [39, 40] that prevents the explicit computation of the divergence of the mobility matrix have been developed; the predictor step reads:

$$r^{\mathrm{P}} = r + \Delta t \zeta_U^{-1}(r)F^{\mathrm{B}}(r) + \Delta t\, \zeta_U^{-1}(r)F^{\mathrm{ext}}(r) \tag{70}$$

The corrector step reads:

$$r^{\mathrm{c}} = r + \frac{\Delta t}{2}\left(\zeta_U^{-1}(r^{\mathrm{P}}) + \zeta_U^{-1}(r)\right)F^{\mathrm{B}}(r)+$$
$$+ \frac{\Delta t}{2}\left[\zeta_U^{-1}(r)F^{\mathrm{ext}}(r) + \zeta_U^{-1}(r^{\mathrm{P}})F^{\mathrm{ext}}(r^{\mathrm{P}})\right] \tag{71}$$

In Eqs. (70)-(71) we have defined the Brownian force $F^{\mathrm{B}}(r) = \sqrt{2k_BT}\zeta_U^{\frac{1}{2}}\frac{\Delta W}{\Delta t}$, with ΔW a discrete increment of a vectorial Wiener process [41]. The covariance of the Brownian force is trivially given by:

$$\langle F^{\mathrm{B}}(r)\left(F^{\mathrm{B}}(r)\right)^T\rangle = \frac{2k_BT}{\Delta t}\zeta_U(r) \tag{72}$$

Therefore it is straightforward to show that:

$$\zeta_U^{-1}(r)\langle F^{\mathrm{B}}(r)\left(F^{\mathrm{B}}(r)\right)^T\rangle\zeta_U^{-1}(r) = \frac{2k_BT}{\Delta t}\zeta_U^{-1}(r) \tag{73}$$

Performing a Taylor expansion of $\zeta_U^{-1}(r^{\mathrm{P}})$ around r, it is straightforward to show that Eqs. (70)-(71) reproduce, in a weak sense (i.e. in expectation),

the divergence of the mobility matrix with respect to the particle positions, i.e. the non-local drift term in Eq. (68). Note that both in the predictor and corrector step the same Δt and, particularly, the same Brownian force vector $F^{\mathrm{B}}(r)$ must be used; it is, however, possible to change the timestep length in the next steps.

To avoid the computation of the divergence of the mobility matrix, we choose to adopt the above predictor-corrector scheme. We have, however, to make connection between quantities appearing in Eqs. (70)-(71) and those appearing in our fluctuating hydrodynamics discretization (see for example Eq. (49)). The external force $F^{\mathrm{ext}}(r)$ is trivially the generalized force vector g, hence, $F^{\mathrm{ext}}(r) = g$. While, in Appendix A (Eqs. (111)-(113)) we show that the quantity $\frac{1}{\sqrt{\Delta t}}\chi(r)\hat{I}$, and $\zeta_U^{-1}(r)F^{\mathrm{B}}(r)$ have the same statistical properties, i.e., zero mean and same covariance. Rescaling $\hat{I}$ by $\frac{1}{\sqrt{\Delta t}}$, the solution of the linear system Eq. (49) gives directly the predictor velocity (see Eq. (60)):

$$U^{\mathrm{p}} = \frac{1}{\sqrt{\Delta t}}\chi(r)\hat{I} + \zeta_U^{-1}(r)g = \zeta_U^{-1}(r)F^{\mathrm{B}}(r) + \zeta_U^{-1}(r)F^{\mathrm{ext}}(r) \qquad (74)$$

and can be used directly for the predictor step. In addition, we also define a corrector velocity:

$$U^{\mathrm{c}} = \zeta_U^{-1}(r^{\mathrm{p}})F^{\mathrm{B}}(r) + \zeta_U^{-1}(r^{\mathrm{p}})F^{\mathrm{ext}}(r^{\mathrm{p}}) \qquad (75)$$

With these definitions, the predictor-corrector Eqs. (70)-(71) assume the compact form:

$$r^{\mathrm{p}} = r + \Delta t\, U^{\mathrm{p}} \qquad (76)$$

$$r^{\mathrm{c}} = r + \frac{\Delta t}{2}(U^{\mathrm{p}} + U^{\mathrm{c}}) \qquad (77)$$

We emphasize that the predictor particle velocity vector U^{p} can be computed by solving the FEM system Eq. (49) (with the particles at positions

26

r and rescaling $\hat{I}$ by $\frac{1}{\sqrt{\Delta t}}$), and has the appropriate statistical properties. The computation of the corrector velocity U^c, instead, involves the product of the mobility matrix evaluated at the predictor positions $\zeta_U^{-1}(r^p)$ and the fluctuating force $F^B(r)$ evaluated at the positions r (i.e. acting on the particles during the predictor step). To accomplish this task, we compute the fluctuating force $F^B(r)$ acting on each particle during the predictor step and subsequently apply such force to the particles in the corrector step.

The fluctuating force $F^B(r)$ can be computed from the force balance:

$$F^B(r) = -F^D(r) - F^{\text{ext}}(r) \tag{78}$$

In the above equation the external force is known, whereas the drag force has to be computed. The drag force $F^D(r)$ is obtained as the reaction force of the fluid on the particles by solving the Stokes equations with a prescribed velocity U^p on the particles, which is exactly that obtained in the predictor step, and with no fluctuation in the fluid.

Finally, in order to compute the corrector velocity U^c, we solve Eq. (49), considering the particles at the predictor positions r^p, with no fluctuations in the fluid (i.e. $\hat{I} = 0$), and with the total force $g = F^{\text{ext}}(r^p) + F^B(r)$ acting on each particle; that is to say:

$$\begin{bmatrix} S & A^T & 0 \\ A & 0 & B \\ 0 & B^T & 0 \end{bmatrix} \cdot \begin{bmatrix} u \\ \Lambda \\ U^c \end{bmatrix} = \begin{bmatrix} 0 \\ 0 \\ F^{\text{ext}}(r^p) + F^B(r) \end{bmatrix} \tag{79}$$

Indeed according to Eq. (60) the particle corrector velocity vector U^c computed with this scheme fulfills Eq. (75).

In summary, our time integration algorithm consists of the following steps:

27

1. At the beginning of each timestep, first solve the FEM system (Eq. (49)) to obtain the predictor step particle velocities U^{p}.

2. Solve the Stokes problem with no fluctuation in the fluid, prescribing the velocities U^{p} computed at the previous point on the particle boundaries.

3. Compute the drag force $F^{\mathrm{D}}(r)$ acting on each particle. The fluctuating force is, then, obtained from the force balance: $F^{\mathrm{B}}(r) = -F^{\mathrm{D}}(r) - F^{\mathrm{ext}}(r)$ (Eq. (78)).

4. Update the particle positions according to the predictor step: $r^{\mathrm{p}} = r + \Delta t\, U^{\mathrm{p}}$.

5. Move the particles to the predictor positions r^{p}.

6. Solve Eq. (79) considering the particles at the positions r^{p}, with no fluctuations occurring in the fluid ($\hat{I} = 0$), considering the particles subjected to the force $g = F^{B}(r) + F^{\mathrm{ext}}(r^{\mathrm{p}})$. From the solution we obtain the particle corrector velocity U^{c}.

7. The final particle displacement is, then, obtained from: $r^{\mathrm{c}} = r + \frac{\Delta t}{2}(U^{\mathrm{p}} + U^{\mathrm{c}})$.

The presented algorithm, being equivalent to Eqs. (70)-(71), represents a first order weak time integration algorithm. We emphasize that our integration algorithm requires updating the boundary fitted mesh according to the particle displacements, the mesh movements details are discussed in the next subsection. We would also like to remark that three Stokes solves are required for each timestep; one to compute the particle predictor velocity U^{p}, one to compute the fluctuating force $F^{\mathrm{B}}(r)$ and another one to compute the corrector velocity U^{c}. We emphasize that when using iterative methods to solve the

three Stokes problems, the CPU time needed for each problem might be quite different due to the availability of effective preconditioners. For example, the computation of the fluctuating force $F^{\mathrm{B}}(r)$ involves an unconstrained Stokes solve, which might be considerably faster than the other two steps. Note that in literature more efficient time integration algorithms have been developed in the context of force coupling method [31] and immersed boundary method [9]; these require a single Stokes solution per timestep. Numerical optimization of the presented algorithm, perhaps adapting the above mentioned ideas to our FEM implementation, will be the object of future work.

4.1. Mesh movements and remeshing

In our boundary fitted mesh implementation, whenever the particles are displaced, the mesh nodes have to be moved resulting in mesh deformation. To guarantee a smooth mesh deformation, we compute the node displacements by solving a Laplace equation [42]:

$$\nabla \cdot (\epsilon \nabla \boldsymbol{d_g}) = \boldsymbol{0} \tag{80}$$

with boundary conditions:

$$\boldsymbol{d_g} = \Delta \boldsymbol{r}_i \quad \text{on the particle boundaries} \quad \Gamma_{\mathrm{p}i} \tag{81}$$

$$\boldsymbol{d_g} = \boldsymbol{0} \quad \text{on the external boundaries} \quad \Gamma \tag{82}$$

In Eq. (80), $\boldsymbol{d_g}$ is the mesh displacement field, the parameter ϵ is taken equal to the inverse of the local element area (in 2D) or volume (in 3D), so that the largest elements adsorb the most part of the deformation [42]. The boundary condition Eq. (81) states that the mesh displacement on the boundary of the i-th particle is equal to the displacement of the particle $\Delta \boldsymbol{r}_i$, whereas Eq. (81)

29

expresses that the nodes on the external boundaries are fixed. Eq. (80) is discretized with standard FEM techniques and the resulting linear system is solved using PARDISO [36].

As the mesh deforms during the simulation, the elements may become extremely distorted reducing the accuracy of the results. Following Hu et al. [42], we use the following parameters to evaluate the mesh quality:

$$m_1 = \max_{1 \leq e \leq N_e} (m_1^e) \quad \text{and} \quad m_2 = \max_{1 \leq e \leq N_e} (m_2^e) \tag{83}$$

where N_e is the number of elements of the mesh and:

$$m_1^e = \left| \log \frac{V^e}{V_0^e} \right| \quad \text{and} \quad m_2^e = \left| \log \frac{S^e}{S_0^e} \right| \tag{84}$$

with V^e and V_0^e being the volume (area in 2D) of element e, and its value in the underformed configuration, respectively, and S^e and S_0^e the aspect ratios of element e and its value in the undeformed mesh, respectively. The aspect ratio is define as:

$$S^e = \frac{(l^e)^3}{V^e} \tag{85}$$

with l^e the maximum length of the sides of element e. As soon as one of m_1 or m_2 is greater than 1.39 (i.e. the element volume or aspect ratio becomes four times larger or smaller than its undeformed value), the mesh is considered too distorted and remeshing is performed.

5. Results

In this section numerical results obtained with the present formulation are reported. We first apply the fluctuating hydrodynamics approach to compute the diffusion coefficients of a sphere in a slit channel and in a cylindrical

cavity. The method is then applied to compute the equilibrium distribution of a circle in a rectangular channel under the effects of an external potential.

5.1. Sphere in a Slit Channel

Since the Brownian motion of a single sphere is a well assessed problem in the literature, we choose to apply the fluctuating hydrodynamics finite element method to study the diffusion of a sphere suspended in a quiescent Newtonian fluid initially located in the midplane between two infinite parallel walls $\boldsymbol{r}(0) = \boldsymbol{0}$.

For these conditions, analytical solutions for the drag coefficient have been developed in the limit of small confinements [43]. Numerical results for the drag coefficient [44] are also available up to very high confined geometries.

A schematic representation of the problem is reported in Figure 2. We denote with H the distance between the walls of the channel and with R_p the particle radius. Therefore, the only dimensionless geometrical parameter is the confinement ratio $\beta = 2R_\mathrm{p}/H$.

It is well-known [45] that an unconfined sphere undergoes an isotropic diffusion with the diffusion coefficient given by $D_\mathrm{bulk} = k_\mathrm{B}T/(6\pi\eta R_\mathrm{p})$. Confinement, however, affects the diffusion coefficients on the diagonal of the diffusion tensor, which become lower than the corresponding bulk value [46].

The calculation of the diffusion coefficient $D_x = D_y = D_\parallel$ is performed through the mean square displacement:

$$\langle (\triangle r_x)^2 \rangle = \langle (\triangle r_y)^2 \rangle = 2D_\parallel \delta t \tag{86}$$

where $\triangle r_x$ and $\triangle r_y$ are the displacements along x and y computed by simulating a single timestep and $\langle \cdot \rangle$ denotes averaging over independent realiza-
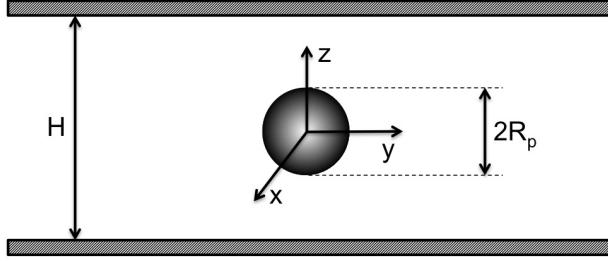
Figure 2: Schematic representation of the problem of a sphere confined between two parallel walls.

tions. We emphasize that, since we are interested only in the first timestep, we can choose an arbitrary small timestep size. Hence, in evaluating the mean square displacement, within a single timestep, the drift term (being linear in Δt) only occurs at order $\mathcal{O}(\Delta t^2)$ and can, therefore, be neglected for an arbitrary small timestep size. The above consideration allows us to neglect the stochastic drift term in Eq. (68) for the computations reported in the present and next section, we can thus use an explicit scheme:

$$\boldsymbol{r}(\Delta t) = \boldsymbol{U}\Delta t \tag{87}$$

and thus:

$$\langle \boldsymbol{r}(\Delta t)\boldsymbol{r}(\Delta t)^T \rangle = \langle \boldsymbol{U}\boldsymbol{U}^T \rangle \Delta t^2 \tag{88}$$

Eq. (88) is the mean square displacement of the particle and can be used to estimate the diffusion coefficient according to Eq. (86) by performing a sufficient number of realizations. Note that the diffusion coefficients are variances themselves; the standard deviation of the estimator of the variance for a normal distribution is $s^2\sqrt{2(N-1)}/N$, with N the number of realizations and s^2 the variance [34].

32

For each confinement ration β, we perform N simulations. The presented approach has two advantages: i) the computation is greatly simplified as the particle does not move and no mesh distortion occurs, ii) the computed diffusion coefficients are assigned to a well-defined point in the space, corresponding to the position of the particle center. We find that $N = 10000$ realizations suffice to get representative results as they produce an accuracy of 1.5% $\pm$ one standard deviation.

In Figure 3 we report the diffusion coefficient $D_\parallel$, normalized with the diffusion coefficient for an unconfined sphere D_{bulk}, as a function of the confinement ratio β (white circles); in the same figure we also report the analytical solution of the normalized drag coefficient [43] (solid line) together with the numerical results for a wider range of confinement values [44] (gray squares).

We point out that a direct comparison between normalized diffusion coefficients (directly calculated by the FH-FEM method) and normalized drag coefficients (computed by hydrodynamic calculations, i.e. imposing a force on the particle and computing its velocity) is allowed as a consequence of the Stokes-Einstein-Sutherland relation. Figure 3 shows that a very good agreement is found with the analytical and numerical results throughout the confinement ratio range considered.

5.2. Sphere confined in a cylindrical cavity

In this section, we employ the fluctuating hydrodynamics finite element method to study the diffusion of a spherical particle in a cylindrical cavity.

A schematic picture of the problem is reported in Figure 4. We denote with H and R the height and the radius of the cylinder, respectively, and with
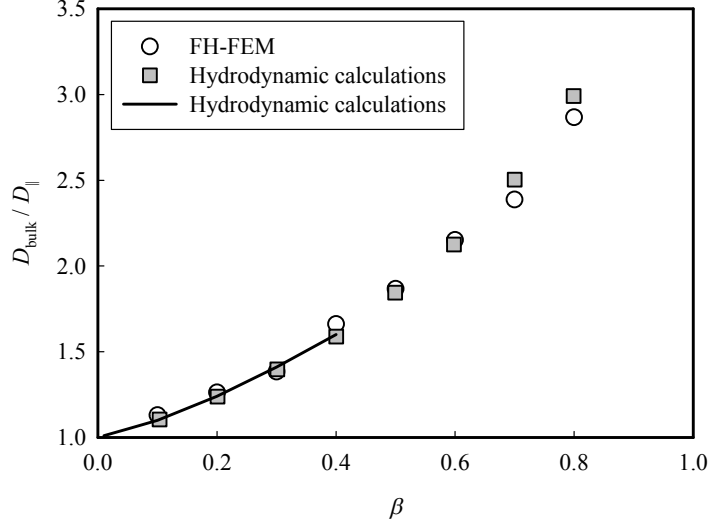
33

Figure 3: Normalized diffusion coefficient of an isolated sphere between two parallel walls in the direction parallel to the walls $D_\parallel$ as a function of the confinement ratio β. The white circles represent our fluctuating hydrodynamics results, gray squares are the numerical solution from [44] and the solid line is the analytical solution from [43]

z, r and θ the axial, radial and angular directions of a reference frame with origin at the cylinder center (see Figure 4). d is the particle diameter and ΔR is the radial distance of the particle center to the cylindrical wall. For this system, the diffusion coefficient have been recently computed [47]. Eral et al. [47] computed the diffusion coefficients along the radial and angular directions, D_r and D_θ, for different distances from the wall, using hydrodynamics calculations, i.e. imposing a force on the particle and computing its velocity.

To make a direct comparison with Eral et al. [47], we choose the radius and the height of the cylinder such that $R = H = 9d$. Furthermore, the
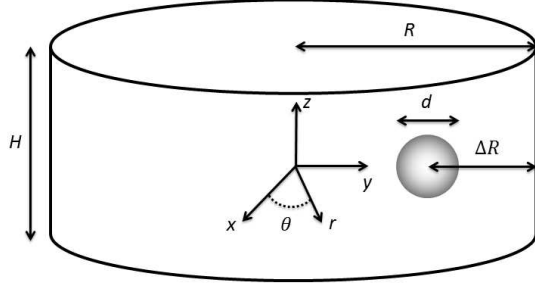
Figure 4: Schematic representation of the problem of a sphere confined in a cylindrical cavity.

particle is initially located on the midplane $z = 0$. We denote with $\xi = \Delta R/d$ the normalized distance from the wall. The calculation of the diffusion coefficients D_r and D_θ is performed through the following equations:

$$\langle (\triangle r_r)^2 \rangle = 2 D_r \Delta t \tag{89}$$

$$\langle (\triangle r_\theta)^2 \rangle = 2 D_\theta \Delta t \tag{90}$$

where $\triangle r_r$ and $\triangle r_\theta$ are the radial and angular displacements computed by simulating a single timestep and $\langle \cdot \rangle$ denotes averaging over independent realizations.

For each of particle wall separations, as we did in the previous section, we compute the displacements by performing only the first step of the FH simulation for a sufficient large number of realizations. The diffusion coefficients D_r and D_θ are computed from Eqs. (88)-(90). Since the diffusion
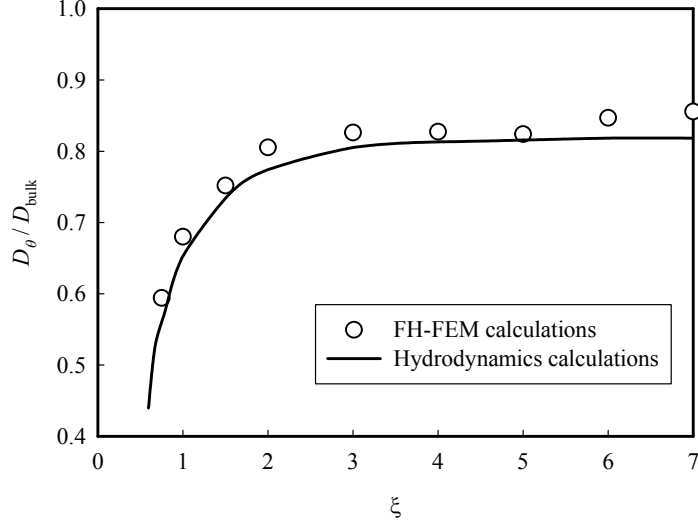
35
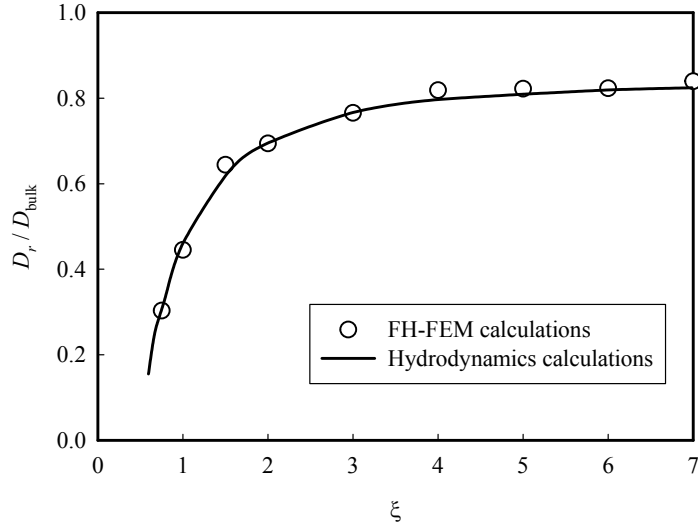
Figure 5: Normalized radial diffusion coefficient D_r as a function of the normalized distance from the cylinder wall ξ. White circles represent our fluctuating hydrodynamics numerical results, the solid line is the diffusion coefficient obtained by Eral et al. [47] through deterministic mobility calculations.

coefficients depend on the particle position, we perform N simulations for each particle-wall distance. In this way the computed diffusion coefficients are assigned to a well-defined point in the space, corresponding to the position of the particle center. With $N = 10000$ realizations for each starting position we get results with an accuracy of 1.5%± one standard deviation.

In Figures 5 and 6, D_r and D_θ, normalized with the diffusion coefficient for an unconfined sphere D_{bulk}, are shown as a function of the normalized distance ξ from the cylinder wall (white circles). Far from the wall, D_r equals D_θ and both are slightly lower than the value D_{bulk} for an unconfined sphere meaning that, even in the region around the cylinder center, the confine-

36

Figure 6: Normalized angular diffusion coefficient D_θ as a function of the normalized distance from the cylinder wall ξ. White circles represent our fluctuating hydrodynamics numerical results, the solid line is the diffusion coefficient obtained by Eral et al. [47] through deterministic mobility calculations.

ment (both radially and axially) still influences the particle diffusion. D_r and D_θ follow a plateau up to $\xi \sim 3$. At smaller distances, the two diffusivities deviate from the constant trend showing a steep decreasing behavior. It appears that D_r is more hindered by the presence of a confinement. In the same figures, the numerical results obtained by Eral et al. [47] computing the drag coefficients through purely hydrodynamics calculations and recovering the diffusivities through the Stokes-Einstein-Sutherland relationship (solid lines). Our numerical results are in excellent agreement with the hydrodynamics calculations.
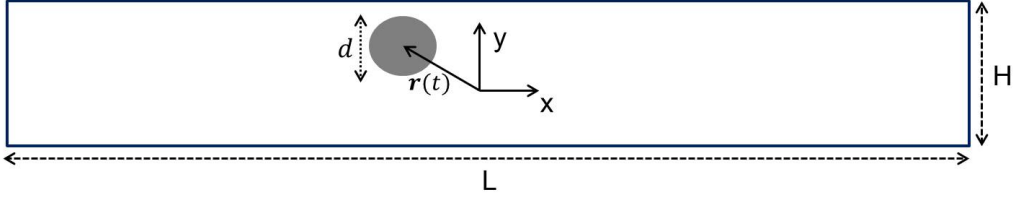
Figure 7: Schematic representation of a circular particle in a rectangular channel.

5.3. Circle in an harmonic potential

In this section we apply the fluctuating hydrodynamics approach to study the trajectories of a Brownian moving circle of diameter d inside a rectangular channel of length $L = 20d$ and width $H = 2d$, under the influence of an external harmonic potential $\Phi(x) = \frac{1}{2}Kx^2$. A schematic representation of the problem is shown in Figure 7, where we denote with $\boldsymbol{r}(t)$ the particle center position vector. A no-slip boundary condition is considered on all the walls of the domain.

It is well known that the equilibrium particle distribution is given by the Boltzmann distribution:

$$P(x, y) = \frac{1}{F} \exp\left(-\frac{\Phi(x)}{k_B T}\right) \tag{91}$$

Where F is just a normalization constant given by:

$$F = \int_{-\frac{H}{2}}^{\frac{H}{2}} \int_{-\frac{L}{2}}^{\frac{L}{2}} \exp\left(-\frac{\Phi(x)}{k_B T}\right) dx dy = H\sqrt{\frac{2\pi k_B T}{K}} \, \text{erf}\left(\sqrt{\frac{K}{2k_B T}} \frac{L}{2}\right) \tag{92}$$

Unlike the previous two examples, in this section we compute the trajectory $\boldsymbol{r}(t)$ employing the algorithm presented in Section 4 to verify if the correct equilibrium distribution is recovered. Indeed, in the present example the diffusion matrix of the particle is a function of its position, due to the presence
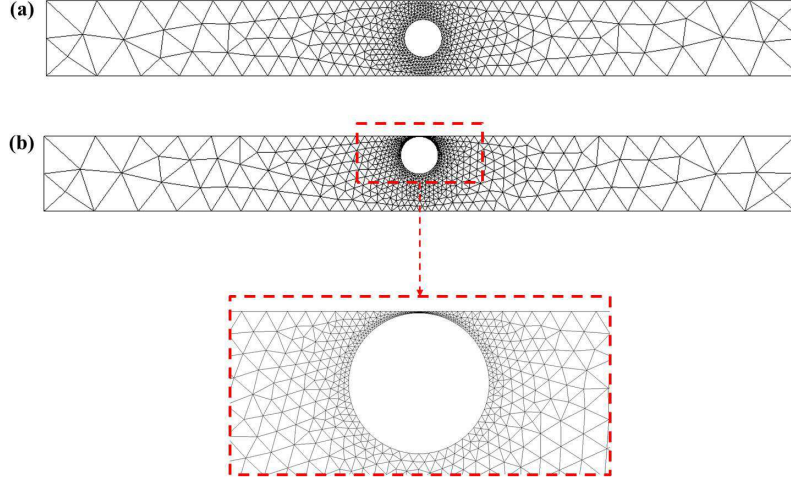
38

Figure 8: (a) Typical initial mesh for the problem of a circle in an harmonic potential, the number of elements is around 1100; (b) typical refined mesh when the circle approaches the wall, the number of elements is around 2000.

of the walls; hence the non-local drift term discussed in Section 4 is non-zero. In our numerical calculations we use a triangular boundary fitted mesh; in order to move the particle inside the fluid domain we use the moving mesh and remeshing algorithm explained in detail in Section 4.1.

Note that, we do not enforce any repulsive potential between the particle and the wall, as a consequence the particle-wall distance can become arbitrary small. We use a meshing algorithm that generates at least five elements between the particle and the wall [48], to ensure that the mesh is convergent even when the particle-wall separation becomes very small. Examples of the initial mesh and of a mesh refined because the circle is very close to the wall are reported in Figures 8a and 8b, respectively.

We perform twelve independent simulations, to compute the particle equi-
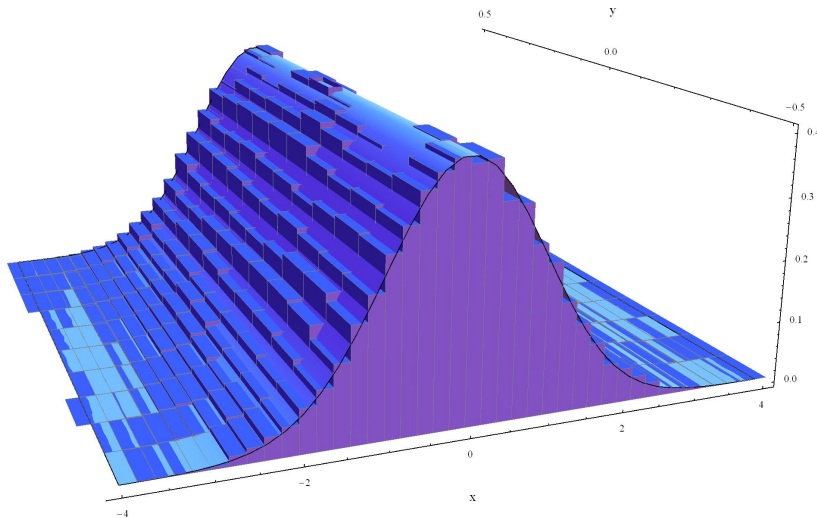
Figure 9: Equilibrium particle distribution, the histogram represent the results obtained from our numerical simulations, the surface is the analytical solution $P(x, y)$ given by Eq. (91).

librium distribution; for each simulation we pick an initial position $\boldsymbol{r}(0) = (x(0), y(0))$ from a uniform distribution in the interval $y(0) \in \left[-\frac{H}{2}, \frac{H}{2}\right]$ and $x(0) \in [-2, 2]$. In each simulation the trajectory $\boldsymbol{r}(t)$ of the particle is computed through the algorithm presented in Section 4. Furthermore to ensure that the equilibrium is reached, every simulation is run to $t = 200\tau$, where $\tau = d^2/D_0$ is the characteristic diffusion time using the diffusion coefficient D_0 of the particle in the center of the channel. We choose a timestep of
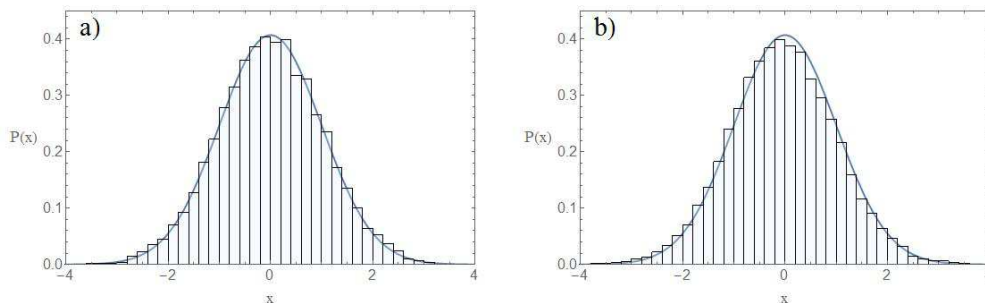
Figure 10: Cross section of the equilibrium particle distribution at two different values of y: a) $y = 0$, and b) $y = \frac{2}{5}H$. The histogram is obtained from our numerical simulations, the solid line is the cross section of the analytical result $P(x, y)$ given by Eq. (91).

$\Delta t = 5 \cdot 10^{-4}\tau$; such a small timestep is required to accurately capture the stochastic drift term in our time integration algorithm also if the particle is close to the walls, where the particle mobility varies strongly.

In order to avoid that a particle overlaps with the walls, we adopt a special adaptive timestep integration algorithm. During the predictor step, if the particle moves outside the domain, we reduce the Δt so that the distance traveled by the particle in the step is 0.95 of the particle wall-separation; the resulting Δt is kept fixed during the subsequent corrector step. Hence, by tuning the Δt we can completely avoid particle-wall overlap events.

In Figure 9 we report the equilibrium distribution histogram obtained from our numerical simulations and the analytical solution $P(x, y)$, where we have chosen the dimensionless parameter $Kd^2/(k_B T) = 1$, to make a further comparison with the analytical solution we also report in Figure 10 two cross sections of the equilibrium distribution histogram at two different values of y. The agreement is perfect, confirming that the time integration algorithm correctly reproduces the drift term required to obtain the Boltz-
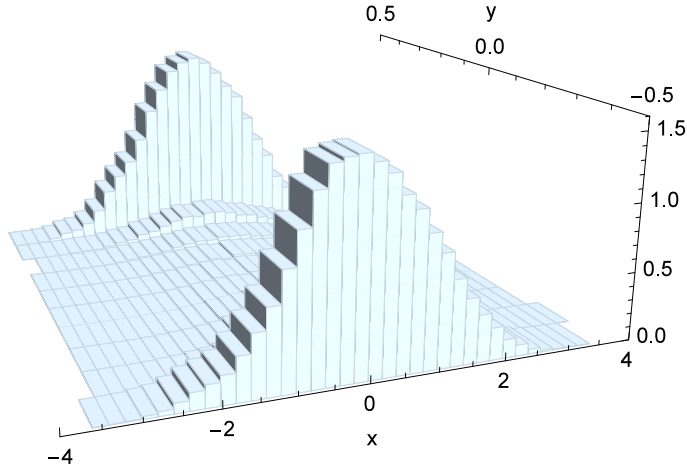
41

Figure 11: Equilibrium particle distribution, the histogram represent the results obtained from our numerical simulations performed neglecting the stochastic drift term in the SDE (Eq. (68)).

mann distribution at equilibrium. As a further verification in Figure 11 we show the equilibrium distribution histogram obtained neglecting the stochastic drift term in the stochastic differential equation (Eq. (68)). To make a more quantitative comparison with the analytical solution $P(x, y)$ we report in Figure 12 two cross sections of the equilibrium distribution histogram at two different values of y. The distribution is clearly different from the analytical solution $P(x, y)$ and shows an erroneous accumulation of particles close to the boundaries.

6. Conclusions

In this work, we have presented a finite element implementation of the fluctuating hydrodynamics according to the Landau and Lifshitz approach. A boundary fitted moving mesh formulation is used for defining the suspended
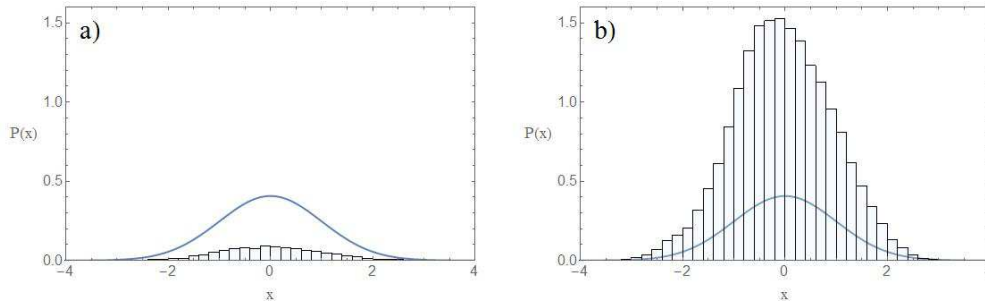
Figure 12: Cross section of the equilibrium particle distribution at two different values of y: a) $y = 0$, and b) $y = \frac{2}{5}H$. The histogram is the result from our numerical simulations performed neglecting the stochastic drift term in the SDE (Eq. (68)), the solid line is the cross section of the analytical result $P(x, y)$.

particles. The proposed implementation fulfills the fluctuation-dissipation theorem exactly at the discrete level as long as the same integration rule is used to discretize the viscous operator and the stochastic forcing. Specifically, the fluctuation dissipation theorem takes the form of a Stokes-Einstein-Sutherland relation between the diffusion coefficient matrix and friction matrix both at the particle and nodal level of the finite elements. The SES relation holds for the general case of curved finite elements of any order. Since fluctuation-dissipation is fulfilled for any mesh, it will be fulfilled for an infinitely refined (converged) mesh as well. To our knowledge, this is the first time that a FEM implementation of the fluctuating hydrodynamics is combined with exact rigid-particle boundary condition, making simulations of arbitrarily shaped particles diffusing in complex confinements possible.

In the present work, we have also presented a multi-step time integration algorithm that correctly reproduces the drift term required in the stochastic differential equation governing the particle positions evolution. This algo-

rithm prevents the explicit computation of the divergence of the particle diffusion tensor, which would be computationally expensive.

The FH-FEM implementation is applied to simulate the Brownian motion of a sphere in slit and in a cylindrical confinement. The numerical prediction for the diffusion coefficient in a slit confinement agree with previous analytical and numerical results. In the cylindrical confinement, the predicted radial and azimuthal diffusion coefficients show a good agreement with experimental measurements and the hydrodynamics calculations.

The time integration algorithm and the FH-FEM is then applied to study the diffusion and the equilibrium probability distribution of a confined circle under an external harmonic potential. The numerically predicted equilibrium distribution perfectly matches the Boltzmann distribution, confirming that the presented algorithm correctly reproduces the drift terms in the SDE.

The present implementation can be extended in several ways. A possible next step is adding inertia both for the fluid and particles. In this case, the extension of our moving mesh algorithm to a complete Arbitrary Lagrangian-Eulerian algorithm is straightforward. Also, the extension of the fluctuating hydrodynamics to deal with complex fluids such as non-Newtonian fluids would be interesting. Future applications will be the study of the Brownian motion of anisotropic particles, such as ellipsoids, possibly under confinement. The Brownian motion of anisotropic particles in different flow fields (such as shear and Poiseuille flow) will be also addressed.

Acknowledgement

We acknowledge the anonymous referees for their valuable comments that significantly improved the paper.

References

[1] L.D. Landau and E.M. Lifshitz. *Fluid Mechanics, vol. 6.* translated from Russian by JB Sykes and WH Reid, 1987.

[2] R. Grima, S. N. Yaliraki, and M. Barahona. Crowding-induced anisotropic transport modulates reaction kinetics in nanoscale porous media. *J. Phys. Chem. B*, 114(16):5380–5385, 2010.

[3] E. Lauga, M. Brenner, and H.A. Stone. Microfluidics: the No-Slip Boundary Condition. In *Springer handbook of experimental fluid mechanics*, pages 1219–1240. Springer, 2007.

[4] L. Joly, C. Ybert, and L. Bocquet. Probing the nanohydrodynamics at liquid-solid interfaces using thermal motion. *Phys. Rev. Lett.*, 96(4):046101, 2006.

[5] T. G. Mason and D.A. Weitz. Optical measurements of frequency-dependent linear viscoelastic moduli of complex fluids. *Phys. Rev. Lett.*, 74(7):1250, 1995.

[6] P. Langevin. On the theory of Brownian motion. *C.R. Acad. Sci.*, 146:530, 1908.

[7] J. F. Brady and G. Bossis. Stokesian dynamics. *Annu. Rev. Fluid Mech.*, 20:111–157, 1988.

[8] M. De Corato, F. Greco, G. D'Avino, and P.L. Maffettone. Hydrodynamics and Brownian motions of a spheroid near a rigid wall. *J. Chem. Phys.*, 142(19):194901, 2015.

[9] S. Delong, F. Balboa Usabiaga, R. Delgado-Buscalioni, B. E Griffith, and A. Donev. Brownian dynamics without Green's functions. *J. Chem. Phys.*, 140(13):134110, 2014.

[10] N. Sharma and N. A. Patankar. Direct numerical simulation of the Brownian motion of particles by using fluctuating hydrodynamic equations. *J. Comp. Phys.*, 201(2):466–486, 2004.

[11] N.A. Patankar. Direct numerical simulation of moving charged, flexible bodies with thermal fluctuations. In *Technical Proceedings of the 2002 International Conference on Modeling and Simulation of Microsystems*, pages 32–35, 2002.

[12] P. J. Atzberger, P. R. Kramer, and C. S. Peskin. A stochastic immersed boundary method for fluid-structure dynamics at microscopic length scales. *J. Comp. Phys.*, 224(2):1255–1292, 2007.

[13] A. J. C. Ladd. Numerical simulations of particulate suspensions via a discretized Boltzmann equation. part 1. theoretical foundation. *J. Fluid Mech.*, 271:285–309, 1994.

[14] M. Serrano and P. Espanol. Thermodynamically consistent mesoscopic fluid particle model. *Phys. Rev. E*, 64(4):046115, 2001.

[15] M. Grmela and H. C. Öttinger. Dynamics and thermodynamics of

complex fluids. i. development of a general formalism. *Phys. Rev. E*, 56(6):6620, 1997.

[16] H. C. Öttinger and M. Grmela. Dynamics and thermodynamics of complex fluids. ii. illustrations of a general formalism. *Phys. Rev. E*, 56(6):6633, 1997.

[17] J. B. Bell, A. L. Garcia, and S. A. Williams. Numerical methods for the stochastic Landau-Lifshitz Navier-Stokes equations. *Phys. Rev. E*, 76(1):016708, 2007.

[18] A. Garcia, J.B. Bell, and S. Williams. Computational fluctuating fluid dynamics. *Math. Model. Num.*, page 1085, 2010.

[19] A. Donev, E. Vanden-Eijnden, A. Garcia, and J. Bell. On the accuracy of finite-volume schemes for fluctuating hydrodynamics. *Comm. App. Math. Comp. Sci.*, 5(2):149–197, 2010.

[20] B. Uma, T.N. Swaminathan, R. Radhakrishnan, D.M. Eckmann, and P.S. Ayyaswamy. Nanoparticle Brownian motion and hydrodynamic interactions in the presence of flow fields. *Phys. Fluids*, 23:073602, 2011.

[21] B. Uma, T.N. Swaminathan, P.S. Ayyaswamy, D.M. Eckmann, and R. Radhakrishnan. Generalized Langevin dynamics of a nanoparticle using a finite element approach: Thermostating with correlated noise. *J. Comp. Phys.*, 135(11):114104, 2011.

[22] R. Radhakrishnan, B. Uma, J. Liu, P. S. Ayyaswamy, and D. M. Eckmann. Temporal multiscale approach for nanocarrier motion with si-

multaneous adhesion and hydrodynamic interactions in targeted drug delivery. *J. Comp. Phys.*, 244:252–263, 2013.

[23] F. Balboa Usabiaga, R. Delgado-Buscalioni, B. E Griffith, and A. Donev. Inertial coupling method for particles in an incompressible fluctuating fluid. *Comput. Methods Appl. Mech. Eng.*, 269:139–172, 2014.

[24] F. Balboa Usabiaga, X. Xie, R. Delgado-Buscalioni, and A. Donev. The Stokes-Einstein relation at moderate Schmidt number. *J. Chem. Phys.*, 139(21):214113, 2013.

[25] E. E. Keaveny. Fluctuating force-coupling method for simulations of colloidal suspensions. *J. Comp. Phys.*, 269:61–79, 2014.

[26] P. J. Atzberger. Stochastic Eulerian Lagrangian methods for fluid–structure interactions with thermal fluctuations. *J. Comp. Phys.*, 230(8):2821–2837, 2011.

[27] P. Plunkett, J. Hu, C. Siefert, and P. J. Atzberger. Spatially adaptive stochastic methods for fluid–structure interactions subject to thermal fluctuations in domains with complex geometries. *J. Comp. Phys.*, 277:121–137, 2014.

[28] H. C. Öttinger. *Stochastic Processes in Polymeric Fluids: Tools and Examples for Developing Simulation Algorithms*. Springer Verlag, 1996.

[29] A.W.C. Lau and T. C. Lubensky. State-dependent diffusion: thermodynamic consistency and its path integral formulation. *Phys. Rev. E*, 76(1):011123, 2007.

[30] S. Delong, F. B. Usabiaga, and A. Donev. Brownian dynamics of confined rigid bodies. *J. Chem. Phys.*, 143(14):144107, 2015.

[31] B. Delmotte and E. E. Keaveny. Simulating Brownian suspensions with fluctuating hydrodynamics. *J. Chem. Phys.*, 143(24):244109, 2015.

[32] R.F. Fox and G.E. Uhlenbeck. Contribution to non-equilibrium thermodynamics. i. theory of hydrodynamical fluctuations. *Phys. Fluids*, 13:1893–1902, 1970.

[33] J.M. Ortiz de Zárate and J.V. Sengers. *Hydrodynamic Fluctuations in Fluids and Fluid Mixtures*. Elsevier, Amsterdam, 2006.

[34] C.W. Gardiner. *Handbook of Stochastic Methods*. Springer Verlag, New York, 1985.

[35] G. Tabak and P. J. Atzberger. Stochastic reductions for inertial fluid-structure interactions subject to thermal fluctuations. *SIAM J. Appl. Mech.*, 75(4):1884–1914, 2015.

[36] O. Schenk and K. Gärtner. Solving unsymmetric sparse systems of linear equations with PARDISO. *Future Gener. Comput. Syst.*, 20(3):475–487, 2004.

[37] H. C. Elman, D. J. Silvester, and A. J. Wathen. *Finite Elements and Fast Iterative Solvers: With Applications in Incompressible Fluid Dynamics*. Oxford University Press (UK), 2014.

[38] F. Brezzi and M. Fortin. *Mixed and Hybrid Finite Element Methods*, volume 15. Springer Science & Business Media, 2012.

[39] M. Hütter and H.C. Öttinger. Fluctuation-dissipation theorem, kinetic stochastic integral and efficient simulations. *J. Chem. Soc. Faraday Trans.*, 94(10):1403–1405, 1998.

[40] M. Fixman. Simulation of polymer dynamics. i. general theory. *J. Chem. Phys.*, 69(4):1527–1537, 1978.

[41] P. E Kloeden and E. Platen. *Numerical Solution of Stochastic Differential Equations*, volume 23. Springer, 1992.

[42] H. H. Hu, N. A. Patankar, and M. Y. Zhu. Direct numerical simulations of fluid–solid systems using the arbitrary Lagrangian–Eulerian technique. *J. Comp. Phys.*, 169(2):427–462, 2001.

[43] J. Happel and H. Brenner. *Low Reynolds Number Hydrodynamics: With Special Applications To Particulate Media*, volume 1. Springer, 1965.

[44] S. Bhattacharya, J. Blawzdziewicz, and E. Wajnryb. Hydrodynamic interactions of spherical particles in suspensions confined between two planar walls. *J. Fluid Mech.*, 541(1):263–292, 2005.

[45] A. Einstein. Motion of suspended particles in the kinetic theory. *Ann. Phys.*, 17(3):549–560, 1905.

[46] L. P. Faucheux and A. J. Libchaber. Confined Brownian motion. *Phys. Rev. E*, 49:5158–5163, 1994.

[47] H.B. Eral, J.M. Oh, D. Van Den Ende, F. Mugele, and M.H.G. Duits. Anisotropic and hindered diffusion of colloidal particles in a closed cylinder. *Langmuir*, 26(22):16722–16729, 2010.

[48] C. Geuzaine and J. F. Remacle. Gmsh: A 3-D finite element mesh generator with built-in pre-and post-processing facilities. *Int. J. Numer. Meth. Eng.*, 79(11):1309–1331, 2009.

A. Proof of the SES relations for the discrete system

From Eq. (49) with only forces f and g and $\hat{I} = 0$, we find that

$$u = S^{-1}f - S^{-1}A^T\Lambda \tag{93}$$

and thus

$$Au = AS^{-1}f - AS^{-1}A^T\Lambda = AS^{-1}f - C\Lambda \tag{94}$$

where we have defined $C = AS^{-1}A^T$. Now with $Au = -BU$ (from Eq. (49)) we find that

$$\Lambda = C^{-1}AS^{-1}f + C^{-1}BU \tag{95}$$

Substituting this expression into Eq. (49) we find

$$B^TC^{-1}AS^{-1}f + B^TC^{-1}BU = g \tag{96}$$

and therefore an explicit expression for U only:

$$U = -D^{-1}B^TC^{-1}AS^{-1}f + D^{-1}g \tag{97}$$

with $D = B^TC^{-1}B$. Now, by using back substitution into Eqs. (95) and (93), respectively, we find expressions for Λ and u:

$$\Lambda = (C^{-1}AS^{-1} - C^{-1}BD^{-1}B^TC^{-1}AS^{-1})f + C^{-1}BD^{-1}g \tag{98}$$

$$u = (S^{-1} - S^{-1}A^TC^{-1}AS^{-1} + S^{-1}A^TC^{-1}BD^{-1}B^TC^{-1}AS^{-1})f$$
$$- S^{-1}A^TC^{-1}BD^{-1}g \tag{99}$$

We can summarize these equations by

$$u = \zeta_u^{-1} f + \chi^T g \tag{100}$$

$$\Lambda = \kappa_u f + \kappa_U g \tag{101}$$

$$U = \chi f + \zeta_U^{-1} g \tag{102}$$

with

$$\zeta_u^{-1} = S^{-1} - S^{-1}A^T C^{-1}AS^{-1} + S^{-1}A^T C^{-1}BD^{-1}B^T C^{-1}AS^{-1} \tag{103}$$

$$\chi = -D^{-1}B^T C^{-1}AS^{-1} \tag{104}$$

$$\kappa_u = C^{-1}AS^{-1} - C^{-1}BD^{-1}B^T C^{-1}AS^{-1} \tag{105}$$

$$\kappa_U = C^{-1}BD^{-1} \tag{106}$$

$$\zeta_U^{-1} = D^{-1} \tag{107}$$

where we have used that S is a symmetric matrix (and therefore C and D as well). Note, that ζ_u is the resistance matrix for forces directly on the nodes of the system and ζ_U is the resistance matrix for forces/torques on the additional unknowns (velocities and rotation rates of particles).

The fluctuating system ($f = g = 0$, $\hat{I}(t) \neq 0$) can be found by substituting $\hat{I}(t)$ for f in the system above:

$$u = \zeta_u^{-1}\hat{I}(t) \tag{108}$$

$$\Lambda = \kappa_u \hat{I}(t) \tag{109}$$

$$U = \chi\hat{I}(t) \tag{110}$$

The covariance matrix of U at two different time instants t and t' can be written as

$$\begin{aligned}
\langle U(t)U(t')^T \rangle &= \chi\langle \hat{I}(t)\hat{I}(t')^T \rangle\chi^T \\
&= 2k_B T\chi S\chi^T \delta(t - t')
\end{aligned} \tag{111}$$

From Eq. (104) we find that

$$\chi S \chi^T = (D^{-1} B^T C^{-1} A S^{-1}) \times S \times (S^{-1} A^T C^{-1} B D^{-1})$$
$$= D^{-1} = \zeta_U^{-1}$$

(112)

and thus

$$\langle U(t) U(t')^T \rangle = 2 k_B T \zeta_U^{-1} \delta(t - t')$$

(113)

and thus also

$$D_U = k_B T \zeta_U^{-1}$$

(114)

the SES relation for the *discrete* system with respect to the U vector. It is now not difficult to show that for u and Λ similar results hold, i.e.

$$\langle u(t) u(t')^T \rangle = 2 k_B T \zeta_u^{-1} \delta(t - t')$$

(115)

$$D_u = k_B T \zeta_u^{-1}$$

(116)

$$\langle \Lambda(t) \Lambda(t')^T \rangle = 2 k_B T \xi \delta(t - t')$$

(117)

$$\xi = \kappa_u A^T C^{-1}$$

(118)